Nuclear Instruments and Methods in Physics Research A 340 (1994) 442–457
North-Holland

NUCLEAR
INSTRUMENTS
& METHODS
IN PHYSICS
RESEARCH
Section A

On quality requirements to the barium fluoride crystals

Ren-yuan Zhu *

Lauritsen Laboratory, California Institute of Technology, Pasadena, CA 91125, USA

(Received 31 July 1992; revised form received 6 September 1993)

This report summarizes the quality requirements to the barium fluoride (BaF_2) crystals for constructing a high precision electromagnetic calorimeter at future hadron colliders. The basic property of BaF_2 crystals and the design and performance of a BaF_2 calorimeter are presented. The emphasis of the discussion is in the radiation resistance of the current production BaF_2 crystals. An approach to implement optical bleaching in situ is also presented. By using optical bleaching current production quality BaF_2 crystals could serve as an excellent candidate to construct a precision calorimeter at future hadron colliders.

1. Introduction

Total absorption shower counters made of inorganic scintillating crystals have been known for decades for their superb energy resolution and detection efficiency. In high energy physics, many large arrays of such counters have been assembled for the precision detection of photons and electrons. A recent example is an electromagnetic calorimeter consisting of 12000 large size BGO crystals constructed by the L3 collaboration at LEP in the last decade [1]. The crystal calorimeter has also attracted much attention in high energy physics community proposing experiments for next generation hadron colliders: the Superconducting Super Collider (SSC) in the US [2,3] and the Large Hadronic Collider (LHC) in Europe [4,5].

The physics at future hadron colliders requires a high precision electromagnetic calorimeter (EMC) [6]. As discussed in this report, a uniform light response over crystal length is one of the necessary conditions to achieve the promised high energy resolution for crystals to be operated in the radiation environment at future colliders. Much progress has been made towards the choice of the scintillating crystal and the production of large size crystals. Attention has been concentrated on two fluoride crystals, barium fluoride (BaF_2) [7] and cerium fluoride (CeF_3) [8], and pure CsI crystal [9].

All known large size fast scintillating crystals suffer from radiation damage with its consequence of a reduced light attenuation length [10], and thus a degraded light response uniformity. A crystal to be used for constructing a precision calorimeter thus must have a stable light attenuation length under irradiation. One approach is to improve its intrinsic radiation resistance. For example, the radiation damage of BaF_2 crystal is saturated after certain amount of dose and the rate of spontaneous recovery of its radiation damage is very slow at room temperature. If the saturated light attenuation length is long enough to provide a uniform light response, the BaF_2 crystal would be a good choice.

An alternative approach is to eliminate the radiation damage in situ. For example, if the radiation damage of a crystal is optically bleachable in situ, and its stable light attenuation length under irradiation and optical bleaching is long enough to provide a uniform light response, the crystal would also serve as an excellent candidate. While it is important to continue effort to improve the intrinsic radiation resistance by using the knowledge accumulated in crystal R & D [10], the optical bleaching provides a practical means of using crystals with lower intrinsic radiation resistance.

This report presents basic property of BaF_2 crystals and the expected performance of a BaF_2 crystal calorimeter, with an emphasis on the consequence of radiation damage for large size production quality crystals. The physics and the practical implementation of optical bleaching for BaF_2 crystals are also discussed.

2. BaF_2 calorimeter design and performance

Barium fluoride is a unique high density inorganic scintillator with three emission spectra peaking at 195,

* Work supported in part by U.S. Department of Energy Grant No. DE-FG03-92-ER40701.

SSDI 0168-9002(93)E1007-K

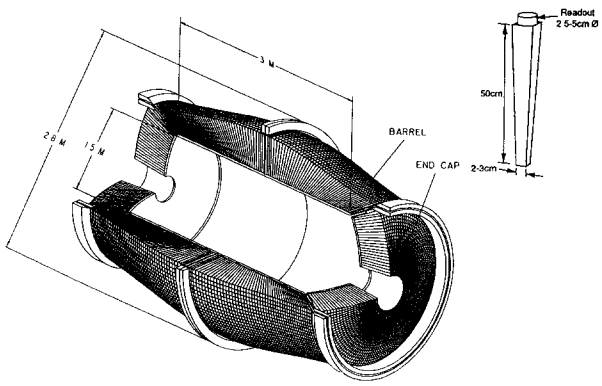

Fig. 1. Conceptual view of a BaF_2 electromagnetic calorimeter.

220 and 310 nm, with decay time constants of 0.87, 0.88 and 600 ns respectively [11]. The intensity of the fast components have no temperature dependence – which should give a BaF_2 calorimeter better intrinsic stability than the L3 BGO calorimeter – while the intensity of the slow component increases with decreasing temperature at a rate of $-2.4\%/°C$ [12]. The speed of the fast components enables a BaF_2 calorimeter to be gated in a single beam crossing at future hadron colliders. Table 1 [8,9,13,14] lists the basic properties of barium fluoride, as compared to other commonly used scintillating crystals: NaI(Tl), CsI(Tl), pure CsI, CeF_3 and BGO. The disadvantage of BaF_2 is a relative longer radiation length, compared to pure CsI and CeF_3 and a higher melting point, compared to pure CsI.

2.1. Design

Fig. 1 shows a conceptual design of a BaF_2 calorimeter, which consists of two parts: a central barrel calorimeter with an inner radius of 75 cm and an outer radius of 140 cm, covering a rapidity range of $|\eta| \leq 1.32$ ($30° \leq \theta \leq 150°$), and two endcaps, located at $z = \pm 164$ cm and covering a rapidity range of $1.32 \leq |\eta| \leq 2.5$ ($9.4° \leq \theta \leq 30°$ and $150° \leq \theta \leq 170.6°$). The total crystal volume of this BaF_2 calorimeter is 10.6 m^3, with a total crystal weight of 51.8 t. Table 2 shows the basic parameters of the BaF_2 calorimeter.

The fine granularity ($\Delta\eta \approx \Delta\phi \approx 0.04$) and hermetic design of the BaF_2 calorimeter provides a uniform response over the phase space coverage and a small (2.7%) dead space which is used for the cable path of a central tracking detector. The detector thickness is 50 cm, i.e. about 25 r.l., which is enough to contain a full shower of high energy electrons or photons.

In addition, the crystals can also be longitudinally segmented to provide a direction measurement for isolated photons. A simple design is to mount two readout devices at two ends of a cell and place a light sealing wall between two segments. Typical segmentation is 8 and 17 X_0. As shown in this report, the BaF_2 calorimeter has the following features.

- Time resolution: gating time in less than 16 ns (a single beam crossing);
- Position resolution: δx and $\delta y \approx 1$ mm at the front surface of crystals;
- Angle resolution: $\delta\theta \approx (50/\sqrt{E} \oplus 8)$ mrad;
- Energy resolution: $(2.0/\sqrt{E} \oplus 0.5)\%$.

We present the time, position and angle resolutions in

Table 1
Properties of some heavy scintillators

	NaI(Tl)	CsI(Tl)	Pure CsI	BaF_2	CeF_3	BGO
Density [g cm^{-3}]	3.67	4.51	4.51	4.89	6.16	7.13
Melting point [°C]	651	621	621	1280	1460	1050
Radiation length [cm]	2.59	1.85	1.85	2.06	1.68	1.12
Molière radius [cm]	4.8	3.5	3.5	3.39	2.63	2.33
Interaction length [cm]	41.4	37.0	37.0	29.9	26.2	21.8
X_{rad}/X_{int}	0.063	0.051	0.051	0.068	0.065	0.051
Refractive index [a]	1.85	1.79	1.95	1.50	1.62	2.15
Hygroscopic	yes	slight	slight	slight	no	no
Luminescence [nm]	410	550	565	310	340	480
(Peak wavelength)			315	220	300	
Decay time [ns]	230	1000	35	630	30	300
			6	0.9	9	
Relative light yield [b]	100	45	4	20	3.5	13
			2	4	3.5	

[a] At the wavelength of the emission maximum.
[b] Relative signal measured with a PMT with a bialkali cathode.

Table 2
Features of the BaF_2 calorimeter

Detector	Barrel	Two endcaps
Rapidity coverage	$\|\eta\| \leq 1.32$	$1.32 \leq \|\eta\| \leq 2.5$
Crystal front/rear face [cm^2])	$3.1\times3.1/5.2\times5.2$	$2.3\times2.3/3.1\times3.1$
Crystal length [cm]	50	50
Crystal number	10880	4144
Crystal volume [m^3]	8.4	2 2
Crystal weight [t]	41.1	10.7

this section. The energy resolution will be discussed in the rest of this report.

2.2. Time resolution

The intrinsic intensity of the slow scintillation component (600 ns) of BaF_2 is 5 times higher than the fast components. Although the slow component may be suppressed in a relatively straightforward way by sampling the output of each channel just before, and a few fast-decay-time constants after the start of a pulse [15], the intrinsic slow component would limit the dynamic range of photosensitive device, and would lead to a pileup noise that degrades the energy resolution.

Direct approaches for suppressing the Slow component have been pursued. An intrinsic suppression was discovered by Schotanus et al. [16]. They found that a small amount of lanthanum added to the crystal during growth greatly suppressed the slow component without significantly affecting the fast component. A subsequent study by Woody et al. [17] showed that there are several dopants which produce strong slow component suppression and retain high fast component light output. However, only lanthanum still preserves the radiation hardness of the pure material up to a level beyond 10^6 rad.

Fig. 2 shows the emission spectra for pure BaF_2 and BaF_2 doped with 1% of lanthanum. The peak intensity of the slow component (310 nm) is reduced by a factor of about five with little change to the fast components (195 and 220 nm).

Since the manufacture of large undoped high quality BaF_2 crystals is inherently simpler, and since the fast and slow scintillation components of BaF_2 peak at different wavelengths, a UV-selective photodevice (optimized for maximum sensitivity in the 220 nm region) is proposed to partially suppress the slow component. The slow component suppression is completed by a fast shaper, and by readout samples just before and shortly after the peak of the pulse. This technique of selecting the fast component does not restrict the dynamic range, and it allows us to maintain very low noise because of the low capacitance of the vacuum photodevice.

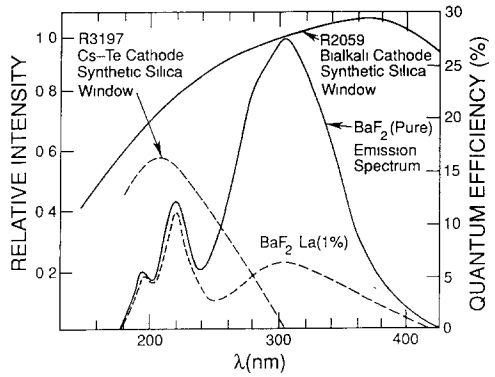

Fig. 2. BaF_2 scintillation spectra and PMT quantum efficiencies.

Fig. 2 also shows the spectral sensitivity of a UV-selective "solar-blind" photomultiplier (PMT) with a cesium telluride (Cs–Te) photocathode (Hamamatsu R3197) compared to a PMT with a bialkali photocathode (Hamamatsu R2059). Both PMTs have a synthetic silica (quartz) window. The Cs–Te photocathode has a quantum efficiency of 10% around 220 nm, while the bialkali photocathode has a quantum efficiency of about 18% around 220 nm. It is clear that the solar-blind photocathode (Cs–Te) is mainly sensitive to the fast scintillation light.

An additional optical suppression of the slow component recently has been achieved by using new photocathodes, K–Cs–Te or Rb–Te, developed by Hammamatsu [18]. Both cathodes have about 10% quantum efficiency at 220 nm and provide better suppression of the slow component (by around a factor of 2 relative to Cs–Te). Fig. 3 shows pictures of the scintillation light pulses recorded on an HP54111D digital scope using a

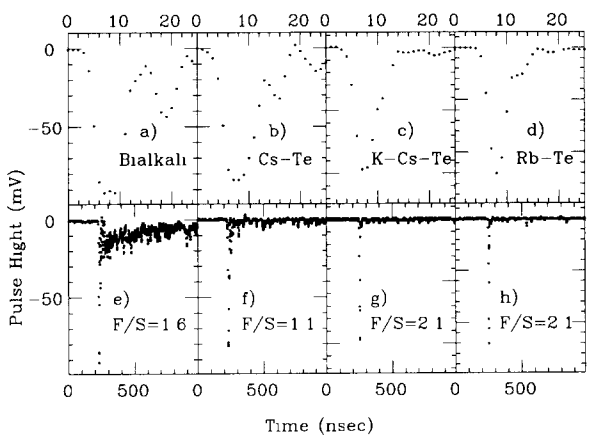

Fig. 3. BaF_2 scintillation light pulse observed by a bialkali cathode (a and e), a Cs–Te cathode (b and f), a K–Cs–Te cathode (c and g), and a Rb–Te cathode (d and h).

bialkali photocathode (a and e), a Cs–Te photocathode (b and f), K–Cs–Te cathode (c and g) and a Rb–Te cathode (d and h). The rise time of the scintillation light pulse in these pictures was completely dominated by the 2.3 ns rise time of the PMTs. On an expanded scale (a, b, c and d) the full width at half maximum of the fast scintillation light is measured to be 4 to 6 ns. The optical suppression factors (F/S) for the slow component, defined as the number of photoelectrons in the fast components (F) divided by the number of photoelectrons in the slow component (S), are also shown in the figure.

An existing photodevice, R4406, may be used in BaF_2 readout. It has quartz window and K–Cs–Te cathode. The triode also has a gain of more than 50% of its nominal value when operating in a 1 T magnetic field with an angle of 45° or less to its axis [19]. Note, the synthetic silica (quartz) window has very high radiation resistance against photon and neutron doses [20]. Another choice of photodevice is proximity focused photomultiplier with fine mesh dynodes, recently developed by Hamamatsu, which has a gain of around 100 under 0.8 T magnetic field.

2.3. Position resolution

The position of an electromagnetic shower without longitudinal sampling, i.e. the coordinate of the impact point of an electron or a photon on the front surface of an electromagnetic calorimeter, is usually measured by using the center of gravity method. The position resolution of a calorimeter thus depends on its structure, especially the lateral cell size. For a calorimeter organized in pointing towers, the position resolution as a function of energy can be parametrized as:

$$\delta x[\mathrm{mm}] = \frac{3}{\sqrt{E}} e^{0.4D}, \tag{1}$$

where E is the energy of the particle being measured in GeV, and D is the cell size in radiation lengths.

A proper lateral cell dimension thus is very important. Its choice is usually a compromise between good position resolution, shower containment in a "tower" consisting of a moderate number of lateral cells, and the total number of readout channels (which is reflected in the cost). Good position resolution as well as a good knowledge of the transverse shower shape (important for e/π resolution) favour a small cell size, while shower containment in a few cells favors a larger size. A cell dimension in the neighborhood of approximately one Molière radius is usually taken, corresponding to $\approx 75\%$ of shower energy deposited in the center cell.

All of these factors taken together have led to a technical consensus that the optimum lateral segmentation is $\approx 0.04 \times 0.04$ ($\Delta\eta \times \Delta\phi$) at the SSC as in the BaF_2 calorimeter design. This segmentation results a position resolution, calculated according to Eq. (1) for a 20 GeV electron or photon, of 1.2 mm, which is comparable to what has been measured with the L3 BGO calorimeter [1].

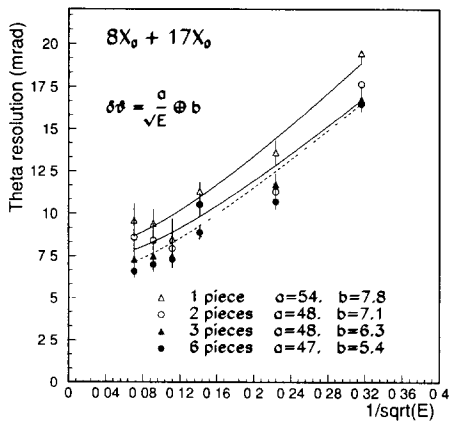

Fig. 4. Angle resolution for a BaF_2 calorimeter with two longitudinal segments.

2.4. Angle resolution

As discussed in ref. [6], it is important to measure the direction of photons with high precision for $H \to \gamma\gamma$ searches. The most accurate measurement of photon direction can be achieved by using the event vertex position determined by the central tracker and the center of gravity of the photon shower. At very high luminosity, however, the efficiency of Higgs vertex determination would be degraded by the pile-up of multi vertices in a single bunch crossing. An alternative method thus is to provide angle measurement with the electromagnetic calorimeter itself, e.g. with longitudinal segmentation, or a position detector.

Fig. 4 shows the angle resolution as function of $1/\sqrt{E}$ for a BaF_2 calorimeter configured with two longitudinal segments of 8 and 17 r.l. The result was obtained by using a full GEANT simulation [21]. The details of the simulation can be found in section 3.3. The angle resolution obtained can be parametrized as

$$\delta\theta[\mathrm{mrad}] = \sqrt{\left(a/\sqrt{E}\right)^2 + b^2}. \tag{2}$$

The result of parametrization is shown in the figure together with result for configurations with the first segment further divided to 2, 3 and 6 pieces. A better angle resolution can be obtained by using three longitudinal segments (4, 5 and 16 r.l.) [21], or a position detector at 5 r.l. [22]. This, however, requires to place a readout device in the middle of a homogeneous calorimeter, which may degrade the energy resolution.

3. Energy resolution

The energy resolution of an electromagnetic calorimeter can be parametrized as:

$$\left(\frac{\Delta E}{E}\right)^2 = \left(\frac{a_0}{E}\right)^2 + \left(\frac{a_1}{\sqrt{E}}\right)^2 + b^2, \tag{3}$$

where a_0 is the contribution from electrical noise, summed over detector readout channels within a few Molière radii around the center of the lateral shower distribution, a_1 is the contribution from the photoelectron statistics, and the systematic term b has three contributions:

$$b^2 = b_G^2 + b_C^2 + b_n^2. \tag{4}$$

Here b_G represents the geometry effect, including shower leakage at the front, side and back of the detector and inactive material between cells. While b_C represents intercalibration error, b_n represents physics noise, including fluctuations and uniformity of response from active media etc.

While terms a_0 and a_1 can be calculated analytically for a total absorption calorimeter, terms b_G, b_n, and term a_1 for a sampling calorimeter, must be studied with realistic GEANT [23] simulations. If the systematic effects from b_n and b_C are under control, a GEANT simulation on energy deposition in the active media provides the best resolution an EMC can achieve.

3.1. Light yield: a_1

It is not very difficult to build a homogeneous electromagnetic calorimeter with a small a_1 term. A photoelectron (p.e.) yield of better than 10 p.e./MeV would be enough to provide an $a_1 = 1\%$. Fig. 5 shows the measured ^{137}Cs spectra obtained from the same BaF_2 sample by using four PMTs with different photocathode (bialkali, Cs–Te, K–Cs–Te and Rb–Te) for two different gate widths (55 ns and 2 μs). Measurements at Caltech show that more than 50 p.e./MeV are obtained from typical 25 cm long BaF_2 crystals by using K–Cs–Te photocathodes.

The light yield of 50 cm long crystals has been measured at Caltech with a ^{137}Cs γ-ray source and at Fermilab with electron beam [24]. For production quality BaF_2 crystals of 50 cm length, the photoelectron yield was measured to be 20 to 50 p.e./MeV by using K–Cs–Te or Rb–Te photocathode. This corresponds to an a_1 term of about 0.4 to 0.7%.

3.2. Electrical noise: a_0

Because of its small capacitance (10 pF) and small dark current (0.1 nA), it is not difficult for an R4406 vacuum phototriode and a front electronics to provide an electrical noise level of 2000 electrons per channel [25]. In reality, one needs to sum over a few Moliere radii to reconstruct an electromagnetic shower. In the case of using 3×3 crystals, which contains more than 93% of shower energy according to GEANT simulations [26], the intrinsic electrical noise is 6000 electrons without channel-to-channel correlations.

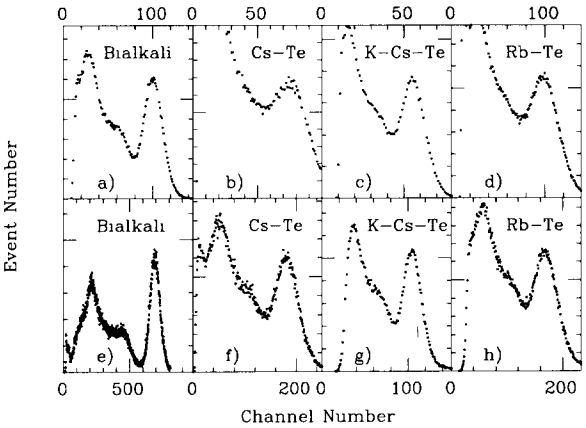

Fig. 5. ^{137}Cs spectra measured with 4 PMTs with different photocathode for two different gate widths: 55 ns (a–d) and 2 μs (e–h).

Assuming the minimum gain of an R4406 phototube is 6, i.e. 50% of its nominal gain of 12 in the worst magnetic field situation [27], the signal corresponds to 120000 to 300000 electrons/GeV with a K–Cs–Te photocathode. This means an a_0 term of 2 to 5% for 3×3 crystal readout. The a_0 term can be further reduced by using recently developed remote processed, proximity photomultiplier tube with fine mesh dynodes. Since it has a gain of up to few hundreds under 0.8 T magnetic field, the a_0 term can be further reduced. The electrical noise introduced by channel-to-channel correlations, however, must be reduced by carefully implementing the electrical isolation between the readout channels.

3.3. Geometry effect: b_G

A detailed GEANT simulation was carried out to estimate the effect of shower leakage and non-active material for the BaF_2 design. It simulated a BaF_2 matrix consisting of 121 (11×11) crystals with the proposed size: 3×3 cm^2 at the front, 5×5 cm^2 at the back and 50 cm long. Effects included in the simulation are: (1) 250 μm carbon fiber wall between crystals, (2) shower leakage because of summing a limited number (3×3 or 5×5) of crystals; and (3) 0.30 radiation lengths of aluminum, representing the beam pipe, the

tracker and the carbon fiber mechanical support, at the front of the BaF_2 array.

Particles were shot uniformly over the front surface of the central crystal of the array. The energies deposited in each crystal, in the carbon fiber walls between crystals, in the aluminum and leaking out sideways were recorded. The result of this simulation for electrons with different energies (5,10, 20, 50, 100, 200 and 500 GeV), in terms of σ of the peak (full width at half maximum (FWHM) divided by 2.35) is listed in Table 3.

3.4. Summary of the energy resolution

Table 3 summarizes the BaF_2 resolution, including contributions from the electrical noise, the photoelectron statistics, the intrinsic resolution from GEANT simulation and the intercalibration. The precision of intercalibration is assumed to be 0.4%, as discussed in section 4. Note, in this table the light response uniformity (b_n) was assumed to be under control. The effect of light response uniformity is discussed in section 5. The result of the energy resolution is shown in Fig. 6b. This resolution can be compared to a simple parametrization of $2\%/\sqrt{E} \oplus 0.5\%$, shown as a solid line in Fig. 6b.

As a comparison, Fig. 6a shows the energy resolution of 4000 BGO crystals (half barrel) obtained in a CERN test beam [1]. In the energy range beyond 20 GeV, the dominant contribution to the energy resolution is the systematic intercalibration uncertainties. The resolution of the L3 BGO calorimeter is also compared to a parametrization of $2\%/\sqrt{E} \oplus 0.5\%$ (solid line).

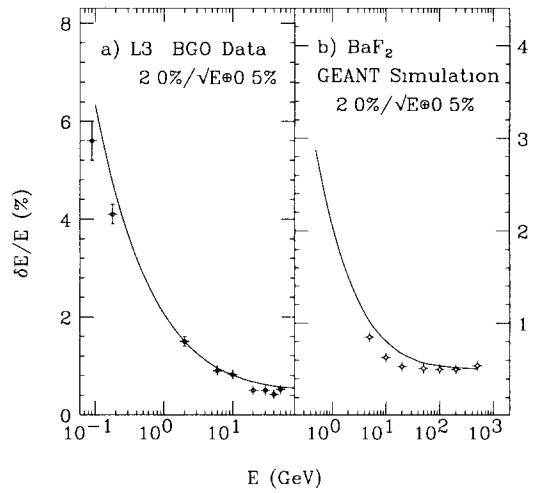

Fig. 6. Energy resolutions of (a) the L3 BGO calorimeter, measured at CERN test beams with 4000 crystals, and (b) a BaF_2 calorimeter, calculated with GEANT simulation. The solid curves represent a simple parametrization of $2\%/\sqrt{E} \oplus 0.5\%$.

4. Intercalibration accuracy: b_C

Precise, frequent calibrations in situ are essential if the high resolution of a precision electromagnetic calorimeter is to be maintained during running. As shown in Table 3, the dominant-contribution to the resolution of a BaF_2 calorimeter at high energies is the uncertainty of the intercalibration. In this section, we discuss two calibration schemes. One uses physics of the collider – calibrate BaF_2 crystals with electrons from Z° decay [28]. The other uses special calibration tools: a Radio Frequency Quadrupole (RFQ) accelerator [29,30] and a xenon UV light flasher [31,32].

In general, the precision of the calibration depends on the intrinsic resolution of the calorimeter itself and the energy range calibrated, compared to the final range of energies to be covered by the experiment. By combining calibration from the Z^0 reconstruction, a UV light flasher system and the RFQ results, a feasible goal is a long term intercalibration accuracy of 0.4%.

4.1. Physics calibration

Inclusive Z^0s are produced copiously at SSC running at the design luminosity. The e^+e^- production from Z decay can be used to provide an accurate intercalibration. The calibration algorithm fits the invariant mass distribution of all Drell–Yan $Z \rightarrow e^+e^-$ events with a Breit–Wigner shape to determine the area (A_{all}), the mass (M_{all}) and the width (Γ_{all}). With a

Table 3
Energy resolution [%] of a BaF_2 calorimeter

E [GeV]	5	10	20	50	100	200	500
Electrical noise	0.4	0.2	0.1	0.04	0.02	0.01	0.004
Photoelectrons	0.2	0.14	0.1	0.063	0.045	0.03	0.02
GEANT (b_G)	0.60	0.43	0.32	0.30	0.30	0.30	0.36
Intercalibration (b_C)	0.40	0.40	0.40	0.40	0.40	0.40	0.40
Total	0.85	0.63	0.53	0.51	0.50	0.50	0.54

fixed width Γ_{all}, the algorithm further fits a similar invariant mass distributions for e^+e^- pairs, which have one electron hits crystal i, to obtain the area A_i and the mass M_i. The $(M_{all}/M_i)^2$ is the correction factor for gain of crystal i after this iteration. The gain of crystals is converged after about 5 iterations. The accuracy of this calibration is statistics limited. With an average of 100 electrons per cell, which can be obtained in about a week at SSC running at the design luminosity, the precision is less than 0.4%.

Fig. 7 shows the initial gains (assuming 10% deviation) and e^+e^- mass spectrum, and the same after the first and the fifth iteration with a statistics of 100 electrons/crystal. It is clear that less than 0.4% accuracy of gain calibration is achieved after 5 iterations.

Studies of monitoring the crystal gains using minimum ionizing particles [33] have shown that a precision of 0.3% can be reached within one to a few hours, using a dedicated trigger at a rate of 1 kHz or more, with small systematic errors.

4.2. RFQ calibration

One novel calibration technique for precision electromagnetic calorimeter is based on an RFQ [29] accelerator. A proton beam accelerated by the RFQ bombards a fluoride target: the reaction $^{19}F(p, \alpha)^{16}O^*$, and the subsequent decay of the excited oxygen nucleus $^{16}O^*$, produces hundreds to thousands of 6 MeV photons per millisteradian per beam pulse at a repetition rate of 30 Hz. These photons, functioning as a synchronized "equivalent high energy photon" of up to 30 GeV per calorimeter cell [34], would serve as a calibration source for SSC electromagnetic calorimeters.

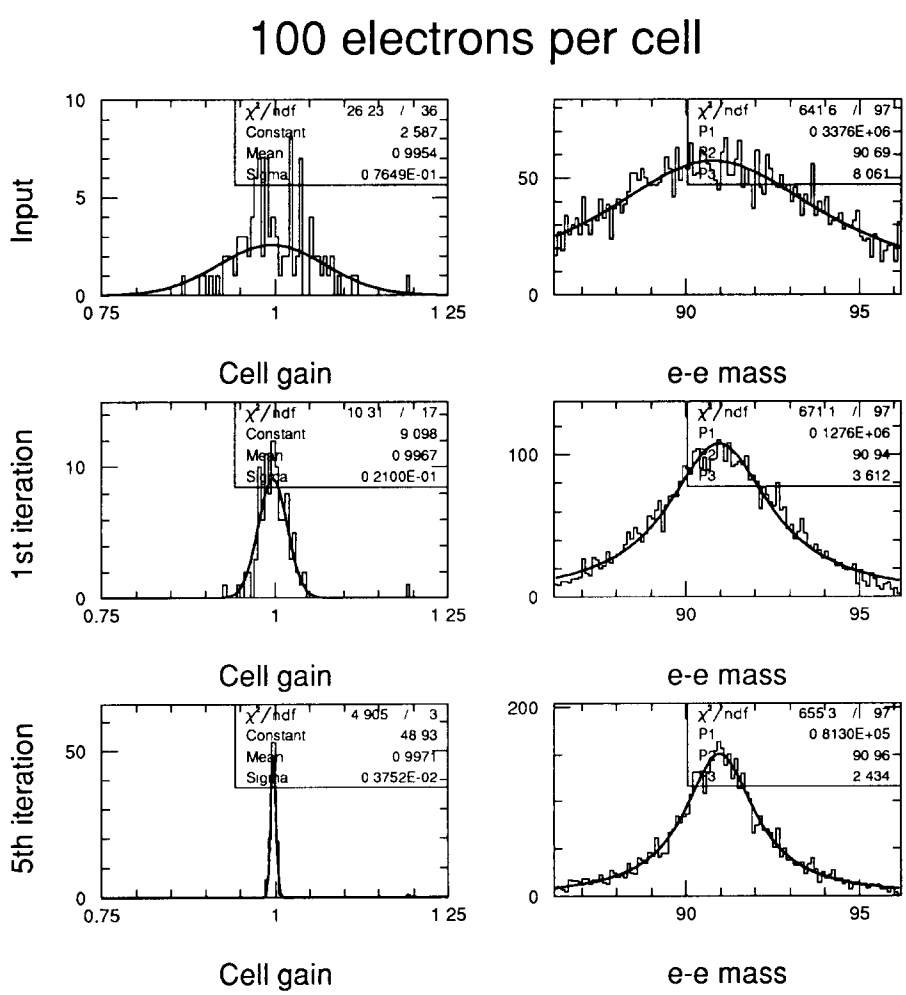

Fig. 7. Crystal gain calibration by using $Z \rightarrow e^+e^-$.

Fig. 8 shows that the deviation of the gain of 49 BGO crystals in a 7×7 test matrix, for several runs [29]. This distribution has a Gaussian shape with a standard deviation of 0.34%, showing that a long term stability of 0.4% is achievable.

The xenon flash lamp monitoring system can be used to monitor the time dependence of a photodetector. The L3 xenon lamp system, which has internal normalization monitors, has been measured [31,32] to be stable to typically 0.2% during 30 d calibration periods in 1990, and to 0.14% over a typical period of 45 d in 1991 during LEP data taking, while the longer-term stability of the entire system is 0.4% to 0.5% per year [32].

5. Effect of light response uniformity: b_n

Experience with the L3 BGO calorimeter [1], and other crystal calorimeters, has shown that light response uniformity at the level of several percent over the length of the crystal (except for the first few and the last few radiation lengths), is important to maintain the resolution. This uniformity is also needed to maintain good linearity over a large dynamic range, e.g. from ~ 10 GeV up to TeV range at the SSC.

Fig. 9 shows the energy fraction (top figure) and the intrinsic energy resolution (bottom figure) calculated by summing energies deposited in a 3×3 BaF_2 crystal array, as a function of light response uniformity.

In this GEANT simulation, the light response (Y) of the crystal was parametrized as a normalized linear function:

$$Y = Y_{25}[1 + \delta(z/25 - 1)], \quad (5)$$

where Y_{25} represents the light response at the middle (25 cm) of a 50 cm long BaF_2 crystal, δ represents the deviation of the light response uniformity, and z is the distance from the small end of a tapered crystal. According to this study, a specification was proposed which requires BaF_2 crystals with a stable light attenuation length (LAL) of longer than 95 cm for production

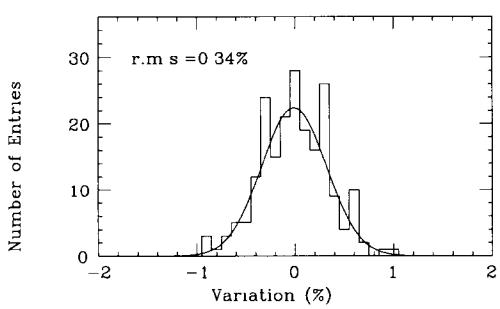

Fig. 8. Variation of the BGO crystal gain calibration.

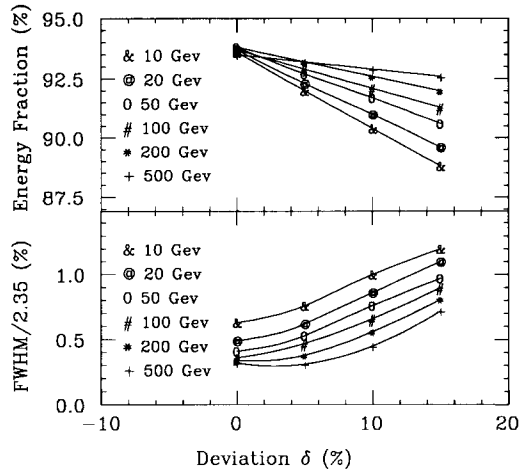

Fig. 9. Effect of light uniformity calculated with GEANT simulation.

(25 cm long) crystals [35], so that the corresponding δ value is less than 5%. Note, the light attenuation length of BaF_2 can be determined by measuring its transmittance [36]. A further study on various different patterns of light response, carried out by Shmakov [37], confirmed this conclusion.

5.1. Light response uniformity measured with 25 cm long crystals

The light response uniformity of BaF_2 crystals can be achieved by using a special wrapping or coating method. For a tapered crystal with its 6 faces polished, there are two complementary factors which affect the light uniformity over the crystal length: the light attenuation and the optical focusing. While the first factor causes a decrease of the response with the increase of the distance to the light-sensitive device, the second factor causes an increase. For a 24 cm long BGO

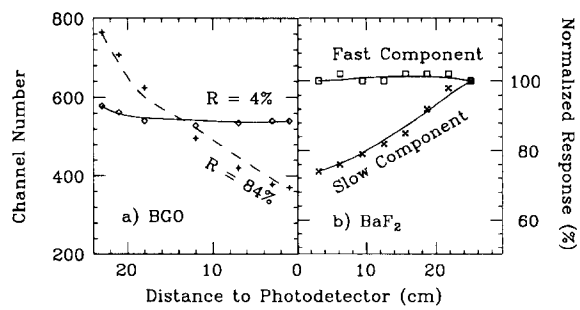

Fig. 10. The light collection responses of (a) L3 BGO crystals and (b) 25 cm long BaF_2 crystals, measured with a collimated ^{137}Cs source running along the axis of the crystals.

crystal, the second factor dominates: a strong increase of light response to the small end was observed for the L3 crystals [1]. Only after extensive studies of controlled depolishing of the surface, was light uniformity and high light collection efficiency achieved by coating the polished BGO crystals with a high reflective NE560 paint layer of 40 to 50 μm thick.

Fig. 10a shows the light uniformity curves with and without the NE560 coating, measured with a ^{137}Cs source. The parameter R in Fig. 10a is the relative light output difference for the source at 21 cm and 3 cm from the readout device. The crosses correspond to an aluminized mylar wrapping and the diamonds to an NE560 coating.

The optical focusing effect, however, is less important for the BaF_2 because of its smaller refractive index. The light collection uniformity of a 25 cm long BaF_2 crystal measured with a collimated ^{137}Cs source is shown in Fig. 10b. The photodetector used in this measurement is a photomultiplier (PMT) with a Cs–Te solar-blind photocathode (Hamamatsu R3197). With simple aluminum wrapping, the measured response of the fast scintillation component shows a uniformity within ~2% in a 25 cm crystal piece. Because of a longer light attenuation length, the response of the slow scintillation component shows an increase with an increasing distance from the PMT, as shown in Fig. 10b.

5.2. *Light response uniformity measured with 50 cm long crystals*

In order to extend the light uniformity results of 25 cm long crystals to a 50 cm long BaF_2 crystal-pair, two important technical difficulties must be overcome: (1) find a glue with good UV transmission down to at least 200 nm. This is needed to optically couple the two crystal pieces together, as well as to couple the crystal-pair to the photodevice; and (2) find a technique of crystal surface treating: wrapping, or UV-reflective coating, to combine good light collection efficiency with overall uniformity.

5.2.1. *KE103 glue*

The best UV-transmitting optical coupling material (down to 190 nm) is Dow Corning 200 Silicone fluid and the GE Silicone based UISC 600M. Although

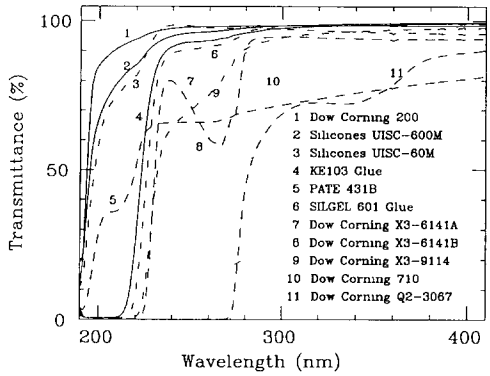

Fig. 11. Transmittance of 500 μm thick layers of various greases and glues.

grease of this type have been used successfully on large BaF_2 crystals in experiments: by Woody at BNL, and by the TAPS Collaboration [38], there is no doubt that a glue is more secure. Following the measurements by Kobayashi et al. at KEK [39], the KE103 (an RTV glue) [40] is chosen as the UV transparent glue. According to ref. [39], the KE103 was also measured to be radiation hard up to a level beyond 10^7 rad.

Table 4 lists the transmission of a thin layer of the KE103 glue, normalized to the Dow Corning 200 fluid. Also shown in the table is the transmission of a thin layer of the GE grease UISC 600M. As shown in the table, the transmission of the KE103 adhesive is nearly as good as the Dow Corning fluid down to 200–205 nm, and shows good transmission down to 195 nm.

However, it should be pointed out that if the layer of the KE103 glue is too thick, e.g. 500 μm, the joint is no longer transparent in UV. Fig. 11 shows the transmittance measured for 500 μm thick layers of various adhesives. The cut-off at 220 nm of KE103 shows clearly that a bad joint of crystal pair would destroy light response uniformity.

5.2.2. *Crystal surface treating*

A simple wrapping technique, in which the region near the phototube is covered with aluminized Mylar painted black to suppress direct light, was used for Fermilab test crystals. The recipe of our wrapping is: 3 to 4 layers of TETRATEX Porous PTFE film (40 μm thick) cover the small end to 24.5 cm, 2 layers of

Table 4
UV transmission [%] relative to Dow Corning 200 fluid

Wavelength [nm]	195	200	205	210	215	220	225	230
KE103/1	87.6	94.5	94.6	97.8	98.3	99.9	99.4	99.4
KE103/2	88.5	95.3	97.6	98.8	99.8	99.4	99.9	99.8
UISC 600M	90.0	94.4	96.4	96.2	97.5	97.3	97.5	97.7

aluminum foil (0.5 mil thick) covers 24.5 cm to 35 cm and 2 layers of aluminized Mylar (25 μm thick) painted black cover the rest of the crystal, i.e. from 35 cm to the large end. This recipe is similar to what used by Winstein et al. at Fermilab and Woody at BNL for BaF_2 wrapping. By adjusting the wrapping, a uniformity at the level of ≈ 5% or better over the length was obtained for 50 cm long BaF_2 crystals with a good glue joint. A result measured at Fermilab with a muon beam hitting a 50 cm long BaF_2 crystal pair transversely is shown in Fig. 12 [24].

Note, the aluminum foil in contact with air is not a high effective reflector for 200 nm light. For the final BaF_2 system, an effective UV reflector, such as MgF_2 with Al overlayer, is to be used as a coating material, as demonstrated by Wuest et al. [41]. We plan to prepare the surface of BaF_2 crystals by using a technique based on a poly-diamond loaded pitch pad with ethylene glycol lubricant. The crystal surface thus produced is virtually free of subsurface defects or an amorphous surface layer, as verified by Rutherford Backscattering at Charles Evans and Associates [41].

6. BaF_2 radiation resistance

The light response uniformity discussed in the last section, however, can not be maintained if the crystal suffers the radiation damage. The deviation of the light uniformity caused by radiation induced color centers destroys the pulse height linearity and the energy resolution. As discussed in section 5, we request a stable light attenuation length of longer than 95 cm for production (25 cm long) BaF_2 crystals under radiation environment at future hadron colliders.

This section discusses the main characteristics and possible mechanism of BaF_2 radiation damage. Unless specified, all crystals tested were produced by Shanghai Institute of Ceramics (SIC) and Beijing Glass Research Institute (BGRI).

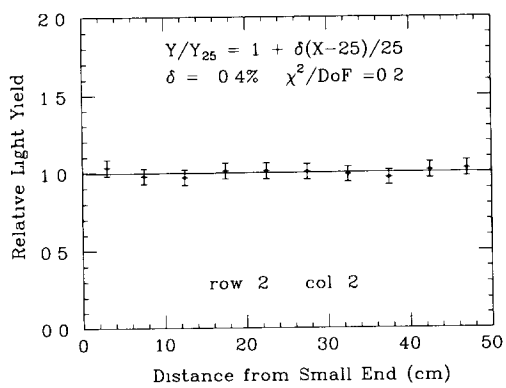

Fig. 12. Light response uniformity of a 50 cm crystal pair measured at Fermilab test beam.

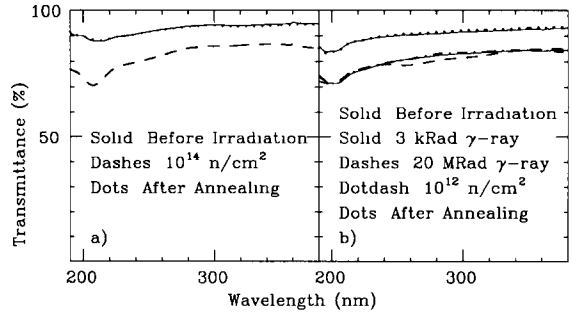

Fig. 13. Transmittances before and after irradiation showing (a) recovery from neutron damage; and (b) typical saturation effect.

6.1. Radiation damage phenomenon

Early test showed that there was no permanent damage caused by either irradiating BaF_2 crystals with photons or thermal neutrons [42]. In addition, all damage recovers in full after a thermal annealing at 500°C for three hours, as shown in Fig. 13. It is also evident that the damage of BaF_2 is caused by the formation of color centers, which introduce a self-absorption of the scintillation light. There seems no apparent damage to the scintillation mechanism itself, so that the intrinsic scintillation light yield by the crystal is not affected [35,43].

The radiation damage of BaF_2 shows clear saturation. Both transmittance and light output measured after irradiation do not degrade further after initial dosage of a few tens to 100 krad, depending on the quality of the BaF_2 crystals. Fig. 14 shows the transmittance of a 25 cm long BaF_2 crystal measured before and after 100, 1k, 10k, 100k and 1M rad irradiation. The saturation is clearly shown in the figure.

It is interesting to note that the net effect of the radiation damage in BaF_2 shows no dose rate dependence. Figs. 14a and 14b show transmittance measured after irradiation with fast and slow dose rate for the same crystal with exactly the same mapping. It is also interesting to note that the spontaneous recovery of the transmittance at 220 nm under room temperature is extremely slow. Fig. 15 shows transmittance measured up to 260 days after 1M Rad irradiation. Also plotted in the figure is the transmittance at 200 and 220 nm as function of time. It is clear that the recovery is indeed at a very slow rate.

All studies above were done for dosage from either γ-rays or thermal neutrons produced by a reactor. In hadron collider, high energy neutrons and hadrons would also be produced. A test by C. Woody showed that a 20 cm long BaF_2 crystal irradiated with $\sim 10^{13}$

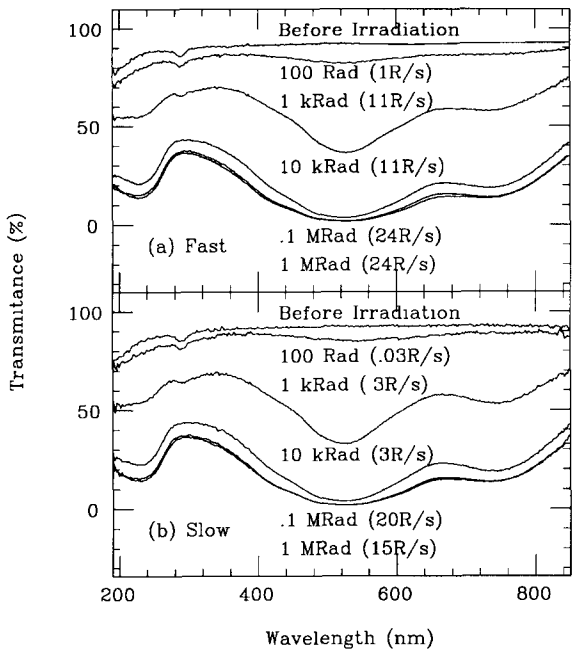

Fig. 14. Transmittance spectra of a 25 cm long BaF_2 crystals before and after ^{60}Co γ-ray irradiation, with dosage of 100, 1k, 10k, 100k and 1M rad for fast (a) and slow (b) dose rate.

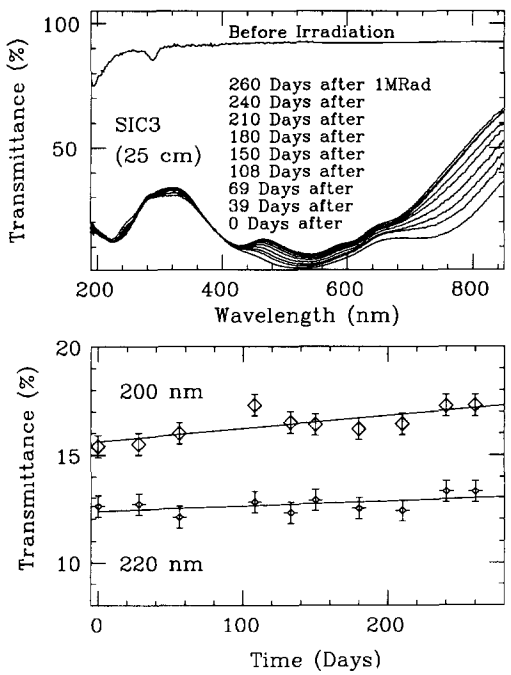

Fig. 15. Transmittance recovery of radiation damage measured under room temperature for a 25 cm long BaF_2 crystal produced in early 1991.

cm^{-2} MeV neutrons at a Van de Graaff facility showed no permanent damage and the level of damage is equivalent to few krad of γ-ray irradiation [43]. Another test by Woody showed that the same crystal irradiated by ~2 Mrad hadrons at AGS facility at BNL also showed no permanent damage and the level of damage is also equivalent to a few krad of γ-ray irradiation [43].

The progress of the radiation resistance of BaF_2 crystals is clearly shown in Fig. 16a where the transmittance of three 25 cm long crystals produced by SIC in early 1991 (SIC102), early 1992 (SIC302) and July 1992 (SIC402) are shown as a function of the wavelength. The light attenuation length of a 25 cm long crystal after saturated damage is 41 cm. Fig. 16b shows the corresponding relative light output before and after irradiation for these three crystals.

Table 5 lists the dimension, transmittance (T) at 220 nm and corresponding light attenuation length (LAL) for these three crystals, where the subscript 0 and 1M refer to before and after 1 Mrad ^{60}Co γ-ray irradiation. The progress in radiation resistance of BaF_2 crystals produced by SIC is clearly shown in the increase of T_{1M} and LAL_{1M}.

Note, the sample SIC402 was irradiated to 1 Mrad by using a ^{60}Co source at SIC, and was consequently bleached to a saturation by using a high pressure mercury lamp whose irradiance spectrum covers 270 to 440 nm. Before the first irradiation, the transmittance of SIC402 was measured at SIC to be 86%.

6.2. Damage mechanism

It is important to understand the mechanism of BaF_2 radiation damage, so that the crystal quality can be improved. This study is a cross disciplinary (high energy physics and material science) research. The BaF_2 project has benefited from the participation of crystal manufactures (SIC and BGRI) and material scientists in the US and China, especially members of the Panel assigned by the SSC laboratory to review the radiation damage problem of BaF_2 [44]. Our understanding of BaF_2 radiation damage mechanism is summarized in this section.

Trace element and micro-structural analysis carried out at Charles Evans and Associates (CE & A) shows that the impurities in BaF_2 are concentrated in some microscopic inclusions, and that there are differences between crystals produced in December 1991 and that from previous batches [45]. The new crystals have much lower Sr concentrations, no detectable rare earths down to typical limits of 0.01 ppm. There are large regions in the new crystals with no inclusions and fewer total inclusions, which are clustered together into macroscopic groups and lie along crystal planes. Study at BGRI shows that crystals produced under poor vac-

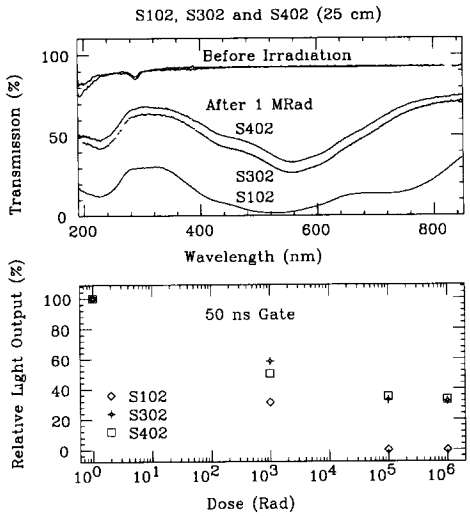

Fig. 16. (a) Transmittance and (b) relative light output of three 25 cm long BaF_2 crystals, produced at SIC in early 1991 (SIC102), early 1992 (SIC302) and July 1992 (SIC402), measured before and after 1 Mrad γ-ray irradiation.

uum have poor radiation resistance [46]. SIC's study shows that a fast cool down leads to a degraded radiation hardness and crystals with more oxygen show larger structural changes under the microscope [47].

A study done by the Tongji group shows OH^- doped crystals, produced through a hydrolysis process by annealing crystal samples in humid air at 900°C, have absorption bands both in the UV and in the infrared, at wavelengths which precisely match those computed for interstitial H and substitutional O^- [48].

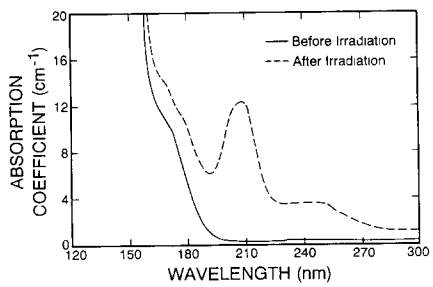

Fig. 17. VUV absorption of an OH^- doped BaF_2 sample.

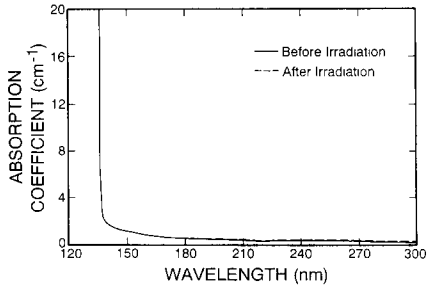

Fig. 18. VUV absorption spectra of a reference BaF_2 sample.

Fig. 17 shows the VUV absorption spectra measured before and after irradiation for an OH^- doped sample. An absorption at 192 nm, caused by hydroxyl center (OH^-) is clearly shown in the spectrum taken before irradiation. The radiation, however, introduced another two absorptions at 206 and 240 nm, which were identified as U and O^- centers.

The Tongji group [48] further suggested that U and O^- centers were formed through a radiolysis process of the OH^- impurity in the BaF_2 crystal:

$$OH^- \rightarrow H_i^0 + O_s^- \quad \text{or} \quad H_s^- + O_i^0, \tag{6}$$

where H_i^0 and O_i^0 are interstitial hydrogen and oxygen atoms, and H_s^- and O_s^- are substitutional hydrogen and oxygen ions. The U center is the product of H^- occupied in a fluorine vacancy. This was further confirmed by an IR absorption at 793.75 cm^{-1} originated from the U center.

As a comparison, the same VUV absorption spectra were taken for a reference sample, which was taken from the same BaF_2 boule, but did not go through hydrolysis or OH^- doping. Fig. 18 shows a very clear UV aborption edge with no radiation induced aborption peaks for this reference sample.

Inspired by the Tongji result, West Va. University studied electron paramagnetic resonance (EPR) spectra obtained with OH^- doped crystals, and observed clearly identified O^- and hydrogen atom signals, which are correlated with the UV absorption bands [49].

All above measurements support the key role of oxygen and hydrogen in combination with other trace impurities, such as rare earths, in BaF_2's radiation damage. A better vacuum and purer raw material thus

Table 5
Properties of three 25 cm long BaF_2 crystals

Sample	Dimension [cm]	T_0 [%]	LAL_0 [cm]	T_{1M} [%]	LAL_{1M} [cm]
SIC102	$3^2 \times 25 \times 4^2$	84.9	418	16.5	15
SIC302	$3^2 \times 25 \times 4^2$	87.2	779	43.3	34
SIC402	$3.6^2 \times 25 \times 4.6^2$	78.4	181	48.6	41

were recommended by the BaF_2 Panel to improve the intrinsic radiation resistance of BaF_2 crystals.

7. Optical bleaching

The improvement of the intrinsic radiation resistance of BaF_2, however, is a very difficult and expensive process. The light attenuation length of 25 cm long BaF_2 crystals after 1M rad of irradiation, achieved in the final meeting of BaF_2 Panel in early August 1992, did not meet the 95 cm specification. As a practical means of applying BaF_2 crystals at the SSC, the panel suggested to implement the optical bleaching [44]. Following Panel's recommendations, five independent measurements on optical bleaching were carried out by BNL [50], Caltech [51], LLNL [52], Tsinghua/McGill University [53] and West Virginia University [49], and were reported in a BaF_2 Expert Group meeting in early September 1992. Based on these studies, the expert group concluded that "the current quality of production crystals available from China is sufficient to meet all GEM specifications as presented to the BaF_2 Panel" [54]. In this section, we discuss this alternative approach of optical bleaching in situ.

7.1. Experiment

Using a calibrated light source from a monochromator, the effect of optical bleaching by using light of different wavelengths was studied [51]. Fig. 19 shows that a blue light of 400 nm is effective in removing color centers in a 25 cm long BaF_2 crystal (SIC302), while a light of 500 nm or longer is not. Fig. 20a shows the transmittance measured at 220 nm as a function of time for another 25 cm long crystal (SIC402) after 1M rad ^{60}Co irradiation and under illumination with 400 nm light from a monochromator which has an intensity of 0.85 mW/cm^2. Before illumination, the transmission at 220 nm was 49%, as shown in Table 5. After illumination, the transmittance recovered to around 78%, corresponding to an LAL of 180 cm. Figs. 20b and 20c show the corresponding LAL and the optically bleachable color center density (D).

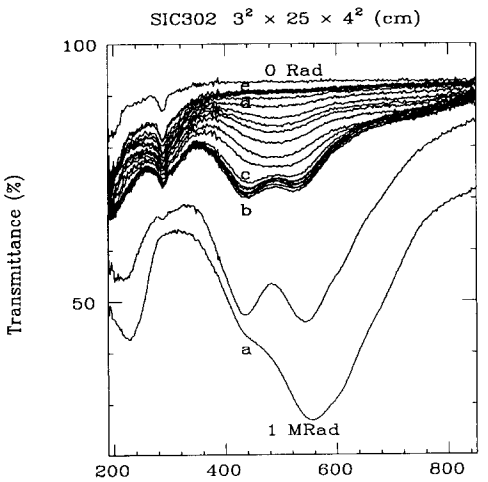

Fig. 19. Transmittance of SIC302 are plotted as a function of wavelength under optical bleaching by light of different wavelengths (a–b: 700 nm, b–c: 500 nm, c–d: 400 nm, d–e: 300 nm).

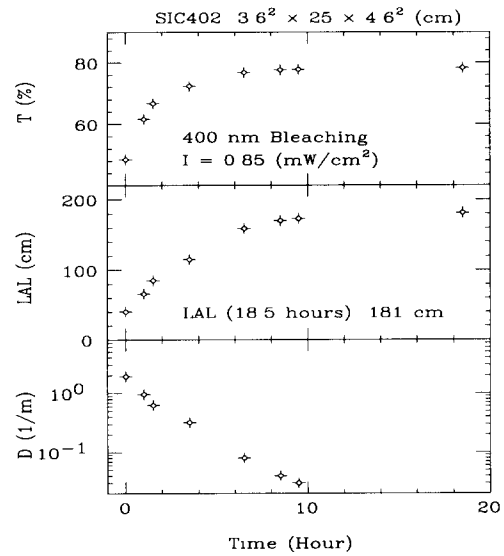

Fig. 20. (a) Transmittance, (b) light attenuation length and (c) bleachable color center density of SIC402 are plotted as a function of time under optical bleaching with a 400 nm light.

A more detailed study looking for the effect of wavelength and initial dosage shows that 450 nm is also effective in removing color centers in BaF_2. The bleaching process can be better parametrized by the sum of two exponentials, i.e. there are two kinds of color centers being formed. Figs. 21 shows the measured bleachable color center density (D) of SIC402 as a function of accumulated energy density (It) of a 450 nm light starting from an initial dosage of 1k (crosses) and 100k rad (diamonds). The parameters of the fit to Eq. (7),

$$D = D_1 \, e^{-a_1 It} + d_2 \, e^{-a_2 It}, \tag{7}$$

are also listed in the figure. It is clear from the figure that the intrinsic annihilation constants a_1 and a_2 and the ratio of the bleachable color center densities D_1/D_2 are independent to the initial dosage. A similar result was observed for crystal SIC302.

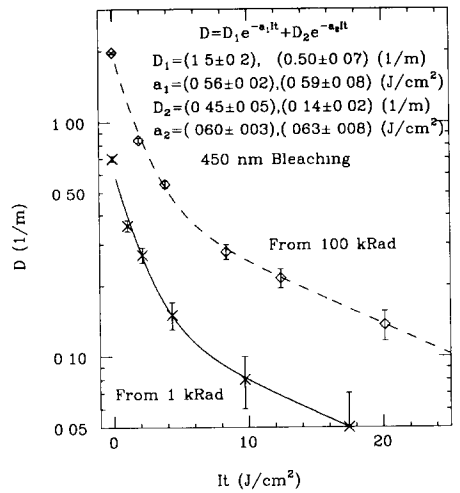

Fig. 21. Bleachable color center density of SIC402 after 1k rad (crosses) and 100k rad (diamonds) irradiation are plotted as a function of energy density of 450 nm bleaching light. The lines are a fit to a sum of two exponentials with parameter listed in the figure.

7.2. Color center dynamics

We have proposed a dynamic model [51] to explain the optical bleaching by color center annihilation and creation. If both processes exist at the same time for one kind of color center, we have

$$dD = -aID\,dt + (D_{all} - D)bR dt, \qquad (8)$$

where D is the optically bleachable color center density, a is annihilation constant in units of $cm^2\ mW^{-1}\ hr^{-1}$, I is the light intensity in mW/cm^2, D_{all} is the total density of traps related to the optically bleachable color centers in the crystal, b is a constant in units of $krad^{-1}$, R is the radiation dose rate in units of krad/h, and t is the time in hours. The solution of Eq. (8) is

$$D = D_0\, e^{-(aI+bR)t} + \frac{bRD_{all}}{aI+bR}[1 - e^{-(aI+bR)t}], \qquad (9)$$

where D_0 is the initial value of the bleachable color center density. For each value of I and of R, an equilibrium between annihilation and creation will be established for one kind of color center at an optical bleachable color center density (D_w) of

$$D_w = \frac{bRD_{all}}{aI+bR}. \qquad (10)$$

According to this dynamic model, the required light intensity to restore the LAL to a stable value of 150 cm (in a dynamic equilibrium) can be estimated for current production BaF_2 crystals to be 10.5 R mW/cm^2.

Table 6 lists the expected radiation dose rate at the front surface of a BaF_2 calorimeter and the corresponding bleaching light intensities required to set LAL = 150 cm at different rapidities, assuming the BaF_2 calorimeter has a barrel of 75 cm radius and two end caps at $z = \pm 150$ cm. A maximum of 150 W is needed to bleach the entire BaF_2 calorimeter at the standard SSC luminosity ($10^{33}\ cm^{-2}\ s^{-1}$).

Table 6
Light intensity needed to maintain BaF_2 at LAL = 150 cm

$\lvert\eta\rvert$	0	1	2.5
Dose rate [krad/h]	0.02	0.04	0.4
I [mW/cm^2]	0.21	0.42	4.2

7.3. Bleaching in situ

Experimental tests have been carried out to verify the color center dynamics described in the previous section. A total of 15 experiments were performed for crystal SIC302. The crystal was irradiated under a uniform ^{60}Co γ-ray source with dose rate of R (krad h^{-1}), and was illuminated with a 450 nm light from a monochromator with an intensity of I ($J\ h^{-1}\ cm^{-2}$) at the same time. Both R and I were varied for different irradiations, but were fixed during a single irradiation. The transmittance and LAL were measured at the end of each irradiation, and were compared to the expected values calculated according to the dynamics. The dose rate R was varied from 0.025 (Run 1–3), 0.1 (Run 4), 0.3 (Run 5) to 0.35 (Run 6–15). The bleaching light intensity I was varied from 4.4 (Run 1–2), 0 (Run 3), 4 (Run 4–5), 3 (Run 6–7), 3.3 (Run 8–9), 0.85 (Run 10–13) to 0.70 (Run 14–15). The duration of these

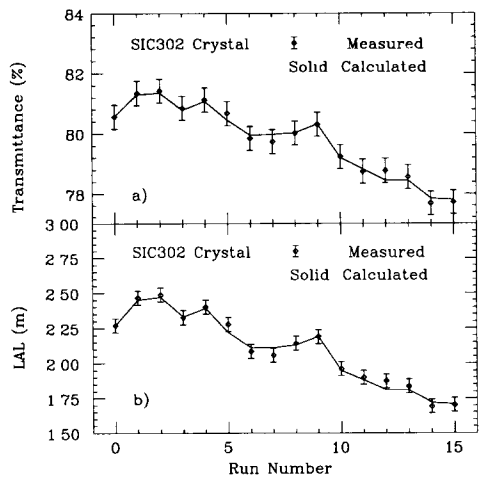

Fig. 22. (a) Measured (points) and calculated (solid line) transmittance and (b) the LAL of crystal SIC302 under ^{60}Co irradiation and 450 nm light illumination.

tests are 1, 4, 2.5, 1, 1, 2.8, 1, 1, 1, 0.75, 1, 1, 1, 3 and 9 hours respectively.

Fig. 22 shows the measured transmittance (a) and LAL (b) (data with error bars) and corresponding calculated LAL (solid line) according to Eq. (9). The parameters a, b and D_{all} are determined from previous measurements: $a = 0.68$ and $0.95\ cm^2\ J^{-1}$ for $D <$ and > 0.08 respectively, $b = 0.65\ krad^{-1}$ for accumulated dose < 5 krad, and $D_{all} = 0.73\ m^{-1}$. The calculated LAL agrees with measured data, which indicates that the color center dynamics discussed in the previous section indeed describes the behavior of the dynamics of radiation damage of barium fluoride crystals.

We are currently investigating practical implementations of optical bleaching in situ. The bleaching light produced by a conventional xenon lamp is coupled to the back face of a 25 cm long crystal through a 2 m long ∅ 6 mm optical fiber system. The initial result is promising. The detailed result will be reported in a future publication.

About 1.6 mW of optical power, integrated in a wavelength region of shorter than 500 nm, is found to be required to set the light attenuation length of the crystal to 170 cm, under a continuous radiation dose of 130 rad/h. The color center behavior with fiber light also obeys the dynamics of Eq. (9). The detailed result will be reported in a future publication.

8. Summary

The construction of a high precision electromagnetic calorimeter at future hadron colliders requires fast scintillating crystals with a stable light attenuation length in a high radiation environment. The requirement for BaF_2 crystals is to have a light attenuation length longer than 95 cm. Although the mass production capability of barium fluoride crystals has been established at SIC and BGRI in China, the improved intrinsic radiation resistance of production size BaF_2 crystals does not yet satisfy the stringent requirement.

An approach to implement optical bleaching in situ has been under investigation. The proposed model of color center dynamics predicts the optical behavior of BaF_2 crystals under irradiation and bleaching. It is expected that the LAL of BaF_2 crystals can be maintained to a required range in situ, so that a precision BaF_2 calorimeter can be constructed with production BaF_2 crystals of existing quality.

References

[1] L3 Collaboration, Nucl. Instr. and Meth. A 289 (1990) 35; and Technical Proposal (May 1983).
[2] L* Collaboration, Letter of Intent to the SSC Laboratory (November 1990)
[3] GEM Collaboration, SSCL SR-1184 (1991)
[4] CMS Collaboration, CERN/LHCC 92-3, LHCC/I1 (1992).
[5] L3P Collaboration, L3P Letter of Intent, CERN/LHCC 92-5, LHCC/I3 (1992).
[6] R.Y. Zhu, GEM TN-91-32 and CALT 68-1777 (1991); R Y. Zhu and H. Yamammoto, GEM TN-92-126 and CALT 68-1802 (1992); S Mrenna et al., GEM TN-93-373 and CALT 68-1856 (1993).
[7] BaF_2 Collaboration, A Precision BaF_2 Crystal Calorimeter for the Superconducting Supercollider, Subsystem R&D Proposal and Progress Report to the SSCL, (1991)
[8] Crystal Clear Collaboration, See S. Anderson et al., Nucl. Instr. and Meth. A 332 (1993) 373.
[9] Z.Y Wei and R.Y. Zhu, Nucl. Instr. and Meth. A 326 (1993) 508.
[10] See papers by Y. Dafinei, D. Hitlin, H. Newman, B. Winstein, C. Woody and R.Y. Zhu, in: Heavy Scintillators, Proc. Crystal 2000 Int. Workshop, eds. F. Nataristefani et al., (Editions Frontieres, 1992).
[11] M. Lavel et al., Nucl. Instr. and Meth. A 206 (1983)169; P. Schotanus et al., Nucl. Instr. and Meth. A 259 (1987) 586; IEEE Trans. Nucl. Sci NS-34 (1987) 76.
[12] P. Schotanus et al., Nucl. Instr and Meth. A 238 (1985) 564; Kobayashi et al , Nucl. Instr. and Meth. A 270 (1988) 106.
[13] Harshow-QS, Scintillation Detectors (March 1992).
[14] BDH Limited, BDH Crystran – Monocrystal Products for Optics, (January 1990).
[15] P. Denes, GEM TN-91-06 (1991).
[16] P Schotanus et al., IEEE Trans. Nucl. Sci NS-34 (1987) 272; Nucl. Instr. and Meth. A 281 (1989) 162
[17] C.L Woody et al., IEEE Trans. Nucl. Sci NS-36 (1989) 536
[18] The K–Cs–Te cathode has been implemented in R4406 triode for BaF_2 readout The Rb–Te cathode has been implemented in R4480 PMT for BaF_2 readout Both tubes use quartz window and are commercially available.
[19] Hamamatsu Photonics K.K., R4406 specification.
[20] S Suzuki, talk given at the Symp. on Detector Research and Development for the SSC, Fort Worth, Texas, October 15–18, 1990.
[21] B.X. Yang and R.Y. Zhu, CALT 68-1907 (1993).
[22] A. Gurtu, in: Proc. 2nd Int. Conf. on Calorimetry in High Energy Physics, Capri, Italy (1991).
[23] R. Brun et al., CERN DD/EE/84-1 (1987).
[24] BaF_2 Collaboration, Beam Test Result of a BaF_2 Matrix, CALT 68-1909 (1993).
[25] The ATT preamplifier has 1200 electron noise for an input capacitance of 10 pF. See M. Levi, in: Symp. on Detector Research and Development for the SSC, Fort Worth, Texas, October 15–18 (1990) p. 3.
[26] R.Y. Zhu, in: ECFA LHC Workshop, Aachen, Vol. 2 (1990) 411.
[27] The nominal gain of R4406 is 4 in the Hamamatsu specification. This low gain, compared to the gain of 12 of Hamamatsu's standard R2148 triode, is due to the processing technology used. At present, the K–Cs–Te cathode has been evaporated inside the closed triode

envelope. This contaminates the dynode, and causes a lower gain because of the lower efficiency of the secondary electron emission from the K–Cs–Te contaminated dynode. This contamination may be eliminated by using a remote processing technology in a large vacuum tank.

[28] R.Y. Zhu, GEM TN-92-143 (1992);
H. Yamamoto, GEM Note in preparation.

[29] R.Y. Zhu, Nucl. Instr. and Meth. A 306 (1991) 145;
H. Ma et al., Nucl. Instr. and Meth. A 274 (1989) 113;
Nucl. Instr. and Meth. A 281 (1989) 469.

[30] R. Hamm et al., An SSC Electromagnetic Calorimeter Calibration Source, Final SBIR Project Report to the Dept. of Energy, AccSys Technology Inc., Pleasanton, California (1991).

[31] W. Ruchstuhl and J. Wenniger, L3 Internal Note 766 (1990).

[32] A. Bay et al., Nucl Instr. and Meth. A 321 (1992) 119.

[33] Y. Kamyshkov et al., Monte Carlo for BaF_2 at ORNL, GEM Progress Report, (1992);
K. Shmakov, GEM TN-143 (1992).

[34] F. Ajzenberg-Selove, Nucl. Phys. A 475 (1987) 1;
H.B. Willard et al. Phys. Rev. 85 (1952) 849.

[35] R.Y. Zhu, CALT 68-1767 (1992).

[36] D.A. Ma and R.Y. Zhu, Nucl. Instr. and Meth. A 333 (1993) 422.

[37] K. Shmakov, GEM TN-92-143 (1992).

[38] W. Doering et al., Total Absorption Photon Spectrometer (TAPS) Collaboration Report No. 3 (1988).

[39] M. Kobayashi et al., Transmittance and Radiation-Resistivity of Optical Glues, KEK Preprint, (1991);
Also see M. Kobabyashi et al., KEK Preprint 90-130, (1990).

[40] KE-103 glue is manufactured by Shin-etsu Chemical Co., Japan.

[41] C. Wuest and B. Fuchs, in: Super Collider 5, ed. P. Hale (Plenum, 1993).

[42] R.Y. Zhu et al., Nucl. Instr. and Meth,. B 61 (1991) 61.

[43] C. Woody, in: Heavy Scintillators, Proc. Crystal 2000 Int. Workshop, eds. F. Nataristefani et al. (Editions Frontieres, 1993) p. 445.

[44] S. Majewski et al., BaF_2 Expert Panel Report, February 1992 and August 1992.

[45] M. Strathman, Report on material chracterization of BaF_2 samples, June–August 1992.

[46] G. Chen et al., in: Supercollider 4, ed. J. Nonte (Plenum, 1992) p. 809.

[47] P.J. Li et al., in: Supercollider 4, ed. J. Nonte (Plenum, 1992) p. 801;
Z.W. Yin, Talk given in East Asia/Pacific – US Symposium on SSC, May 1992.

[48] L.Y. Chen et al., GEM TN-92-129 (1992);
L.M. Wang et al., The Optical and Radiation Damage Properties of Barium Fluoride Crystals, talk presented in Shanghai BaF_2 Workshop, Shanghai, May 1991.

[49] L. Halliburtoon et al., Identification and Chracterization of Radiation-Induced Point Defects in BaF_2, University of West Virginia Optoelectronics Reports (1992).

[50] S.P. Stoll, UV and Visible Light Bleaching of Radiation in SIC BaF_2 Sample 703, BNL Report (1992).

[51] D.A. Ma. and R.Y. Zhu, Nucl. Instr. and Meth. A 332 (1993) 113.

[52] C.R. Wuest and G.J. Mauger, Effects of Light Exposure on Irradiated BaF_2 Crystals, LLNL Report (1992).

[53] R.C. Shang, Optical Annealing of BaF_2 Crystals with Laser Beam, A joint work by R.C. Shang and Optical Group in McGill University (1992).

[54] C. Wuest et al., Report of the BaF_2 Expert Group, September 2, 1992.